Self consistent tight binding model for dissociable water

You Lin, Aaron Wynveen, J. W. Halley, L. A. Curtiss, and P. C. Redfern

Citation: J. Chem. Phys. **136**, 174507 (2012); doi: 10.1063/1.4705667
View online: http://dx.doi.org/10.1063/1.4705667
View Table of Contents: http://jcp.aip.org/resource/1/JCPSA6/v136/i17
Published by the American Institute of Physics.

Self consistent tight binding model for dissociable water

You Lin,[1] Aaron Wynveen,[2] J. W. Halley,[2] L. A. Curtiss,[3] and P. C. Redfern[3]
[1]*Brion Technologies Incorporated, 4211 Burton Drive, Santa Clara, California 95054, USA*
[2]*School of Physics and Astronomy, University of Minnesota, Minneapolis, Minnesota 55455, USA*
[3]*Argonne National Laboratory, Argonne, Illinois 60439, USA*

(Received 27 September 2011; accepted 9 April 2012; published online 3 May 2012)

We report results of development of a self consistent tight binding model for water. The model explicitly describes the electrons of the liquid self consistently, allows dissociation of the water and permits fast direct dynamics molecular dynamics calculations of the fluid properties. It is parameterized by fitting to first principles calculations on water monomers, dimers, and trimers. We report calculated radial distribution functions of the bulk liquid, a phase diagram and structure of solvated protons within the model as well as ac conductivity of a system of 96 water molecules of which one is dissociated. Structural properties and the phase diagram are in good agreement with experiment and first principles calculations. The estimated DC conductivity of a computational sample containing a dissociated water molecule was an order of magnitude larger than that reported from experiment though the calculated ratio of proton to hydroxyl contributions to the conductivity is very close to the experimental value. The conductivity results suggest a Grotthuss-like mechanism for the proton component of the conductivity. © *2012 American Institute of Physics*. [http://dx.doi.org/10.1063/1.4705667]

I. INTRODUCTION

For the study of electrochemical and biological problems at the atomic level, a description of water which is dissociable is essential. For example, one needs to describe hydrolysis by cations, dissociation at oxide surfaces, oxygen reduction processes, and many other reactions involving hydroxyl, hydronium, molecular oxygen, and other species all deriving from the constituents of water. It is extremely artificial to model all these species separately. Full first principles descriptions of dissociable water are available[1] but they are prohibitively expensive to use in simulations also taking account of oxide and metal surfaces or large biopolymers. For these reasons we have been involved in development of dissociable molecular dynamics models of water for a long time.[2,3] The polarizable molecular dynamics used in our earlier work did not take explicit account of electronic structure. The empirical valence bond (EVB) method[4,5] by Warshel and co-workers and used mainly to describe homogeneous reactions in solvents and gas phase, takes some further account of electronic structure. It uses potential surfaces parameterized using first principles calculations for two electronic states relevant to the reaction of interest while treating the solvent as a classical polarizable fluid as in Refs. 2 and 3.

Self-consistent tight binding methods, including the one used in this paper, follow just one adiabatic Born Oppenheimer surface, but take more complete account of the electronic structure of the entire system. In the self consistent tight binding method (SCTB) described here we use a larger first principles database than is usually used in the EVB method and use atomic configurations in the fitting database independent of the configurations encountered in the applications, in order to make the method as predictive as possible. For example, in modeling solids, we use first principles data from atomic configurations for bulk solids and test the predictive quality of the results by simulating surfaces without further fitting as described in Refs. 6–9. In the work described here, we used a first principles derived database of configurations of gas phase clusters for fitting and we test the predictive capability by using the result to simulate the properties of bulk liquid water without further fitting and comparing them to experimental data and to the results of first principles simulations. As we will show, the results are quite good, though, of course, one can obtain a better fit with a classical model which is fit directly to the properties of the liquid. We contend, however, that our SCTB model will be a better predictive tool than such classical models when confronted with situations for which it was not directly fit, such as water/electrode and water/nanoparticle interfaces. We have already used the water model described here for one such study.[10]

Another self consistent tight binding model for water was quite recently reported by Paxton and Kohanoff.[11] The basic physics is very similar but the method for taking account of the polarizability of the oxygen entities in the model differs in some details from the method used here as described in more detail in Appendix A of this paper and in Ref. 6. An advantage of the model reported here is that it has been constructed to be completely compatible with our previous SCTB models of oxides, so that it can be used, as already reported in Ref. 10, to study oxide-water interfaces.

We first used SCTB (Ref. 6) to describe titanium dioxide. We have since used it to describe magnetic materials[12] and metals.[7,8] SCTB is similar to the approach of Refs. 13–15 but differs from it in some details which are important in our applications. In particular, we use no explicit wave functions but parameterize the matrix elements, within the well known Slater two center scheme. We include multipole moments, which have proved vital in several applications. We fit directly to density functional theory (DFT) or Hartree Fock

based methods including Moller-Plesset perturbation theory as used in this work on water. We can include spins and have demonstrated[12] an ability to postdict noncollinear spin structures. There are no classical forces on the atoms (though the environmental terms in the Hamiltonian play a similar physical role to such classical forces in other approaches). A formal mathematical description of SCTB is summarized in Appendix A where references to sources of further details appear.

II. DETERMINATION OF SCTB PARAMETERS FOR WATER

We used a "fitting code" developed previously and capable of fitting first principles results both for clusters and for periodically continued solids with an SCTB parameter set by Monte Carlo search through the parameter space. The code has been used previously and subsequently to generate parameter sets for titanium dioxide,[6] titanium metal,[7] ruthenium dioxide,[9] and platinum metal.[8] The data set which was used for fitting parameters for water included first principles energies for 364 configurations of the water molecule, 1304 atomic configurations of the water dimer (using MP2/6-311+g(3df,2p)) and all the harmonic frequencies of the relaxed water trimer (using MP2/aug-cc-pVDZ and reducing the computed frequencies by a factor 0.95 in the fitting database). The 364 water configurations were the equilibrium structure (O-H = 0.95720 Å and H-O-H = 104.3758°) and 363 monomers generated in O-H_1 and O-H_2 bond ranges from 0.7 to 1.3 Å with step 0.06 Å at scissor angles 100°, 103.3°, and 106.67°. For the dimer, 1215 configurations were generated by using the five O-O distances 4.5, 5.5, 5.58, 6.5, and 7.0 Bohrs and, for each, varying the five angular degrees of freedom each angle taking three values with step size 30°. Eighty nine more configurations were generated in regions where the energies were rapidly varying in order to obtain better defined energy surface for fitting.

During the fit, we calculated the following weighted error and minimized it:

$$\begin{aligned} error = & \sum_{l} w_l \left(E_{SCTB}^{\{bind\}} - E_{FP}^{\{bind\}}\right)^2 \\ & + w_{dipole} \sum_{l \in monomer} w_l (\mu_{SCTB} - \mu_{FP})^2 \\ & + w_{phonon} \sum_{\nu \in trimer} w_\nu (\nu_{SCTB} - .95\nu_{FP})^2 \\ & + w_{phononvect} \sum_{\nu \in trimer} w_\nu (\vec{a}_{SCTB} - \vec{a}_{FP})^2, \quad (1) \end{aligned}$$

where $E_{SCTB/FP}^{\{bind\}}$ are the binding energies of SCTB and first-principles method, respectively; $\mu_{SCTB/FP}$ the molecule dipoles; $\nu_{SCTB/FP}$ the phonon frequencies; $\vec{a}_{SCTB/FP}$ the phonon eigenvectors. The weights are labeled by w, and here is how they are assigned: $w_{phonon} = 10^{-4}$, $w_{phononvect} = 10$, and $w_{dipole} = 20$ are weights for the phonon frequencies and eigenvectors and for the water dipole moment. $\{w_l = 1\}$ are the weights assigned for individual structures and $\{w_\nu\}$ are relative weights assigned for different frequencies. $w_\nu = 1$ for the lower 12 first-principles frequencies and $w_\nu = 0.01$ for highest nine first-principles frequencies. The high frequency modes were deliberately under-weighted to allow a better fit for low frequencies. The unit for energies is eV; dipoles Debye; frequencies cm^{-1}; and phonon eigenvectors are normalized to 1. Since the low frequency modes of the water trimer are hard to distinguish by use of the frequencies alone and one does not want to match the wrong SCTB mode with the first-principles mode, a smaller optimization loop minimizing the trimer error is employed first. The loop minimizes the total error due to trimer normal modes:

$$\begin{aligned} & w_{phonon} \sum_{\nu \in trimer} w_\nu (\nu_{SCTB} - .95\nu_{FP})^2 \\ & + w_{phononvect} \sum_{\nu \in trimer} w_\nu (\vec{a}_{SCTB} - \vec{a}_{FP})^2. \quad (2) \end{aligned}$$

The weights assigned to the high frequency modes of the water trimer were quite low and as a consequence, these modes, including the well known symmetric and asymmetric stretch modes are not fit well by the SCTB model. This choice of weights was chosen so that the model would have good properties at thermal energies, but we caution that it means that near infrared properties are not well reproduced. For the tight binding fits, we started with hydrogen-oxygen parameters given for a somewhat similar water model (which, however, was not self consistent) due to Sankey and co-workers.[16] However, for oxygen-oxygen parameters we used values obtained in our most recent SCTB model of titanium dioxide[10] so that the same model parameters for oxygen could be used later to simulate the water-oxide interface.

The final parameter set is presented in Appendix B. The quality of the fits is illustrated in Figures 1–4 where aspects of the resulting properties for monomer, dimer, and trimer are shown.

III. SCTB RESULTS ON BULK WATER

As a test of the predictive power of the SCTB model resulting from fitting the first principles data on water clusters, we calculated properties of liquid water from the model without further fitting. In Figure 5, we show the results of

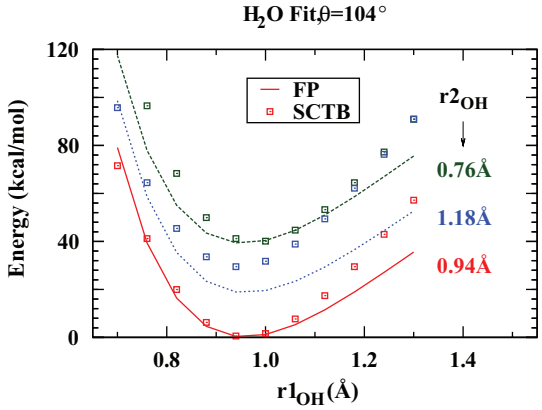

FIG. 1. First principles and SCTB results for energy of a single water molecule. Three values of the scissor angle were simultaneously fit. Here the scissor angle was 103.3°.

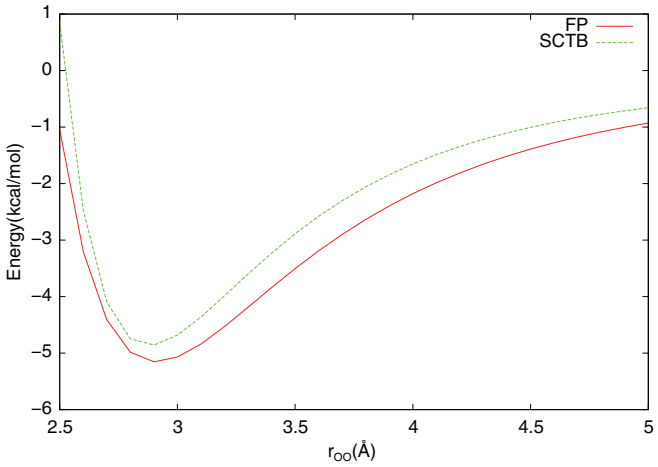

FIG. 2. Energy of the water dimer as a function of the oxygen-oxygen distance after the fit.

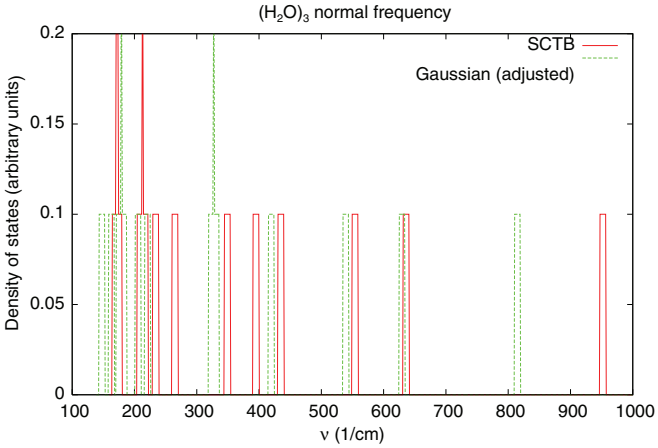

FIG. 3. Comparison of low frequency harmonic frequencies of the water trimer with values from the SCTB model, after the fit. The vertical axis is the density of phonon states.

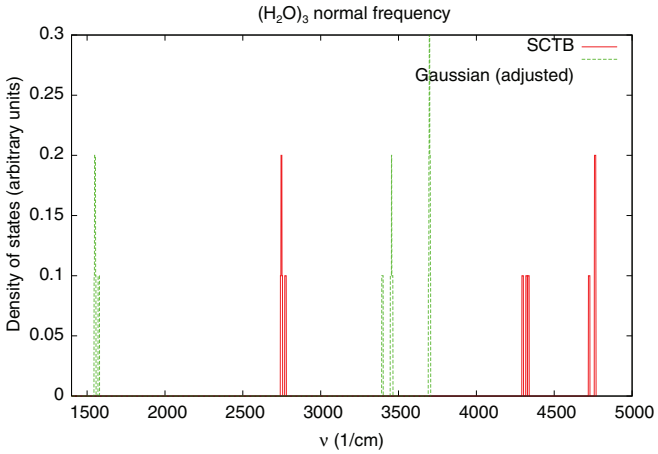

FIG. 4. Comparison of high frequency harmonic frequencies of the water trimer with values from the SCTB model, after the fit. These frequencies were given a low weight in the error function minimized in the fit.The vertical axis is the density of states.

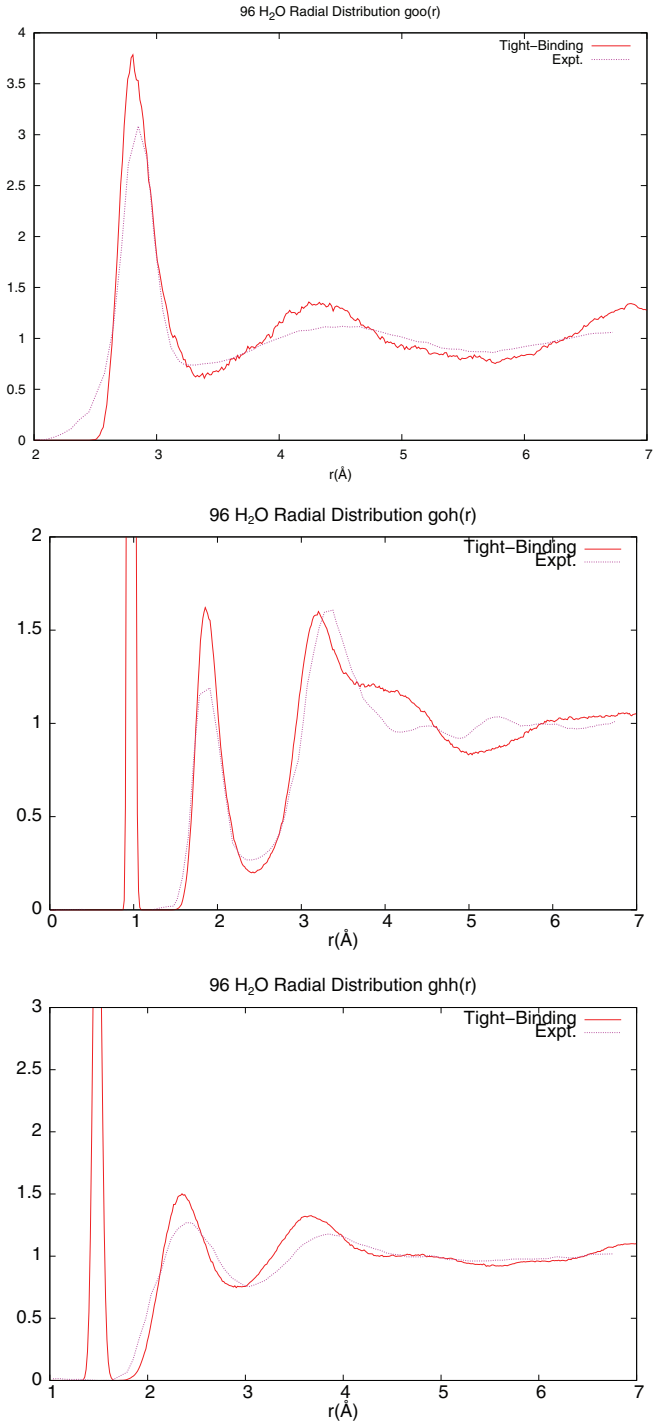

FIG. 5. Radial distribution functions for liquid water calculated (red) from the SCTB model for 96 water molecules with periodic boundary conditions run for 10 ps at 300 K compared with the same quantities (pink) inferred from neutron scattering experiments on liquid water at the same temperature.

calculations using the model for the radial distribution functions of liquid water calculated for 96 molecules by direct molecular dynamics SCTB simulation in which the electronic structure and atomic forces are recalculated after each MD step. For comparison, we show experimental results for the same quantities, derived from neutron scattering data[17] and x-ray scattering data.[18] Hydrogen bonding and tetrahedral oxygen coordination are correctly described. There are some discrepancies between simulation and experiment beyond the

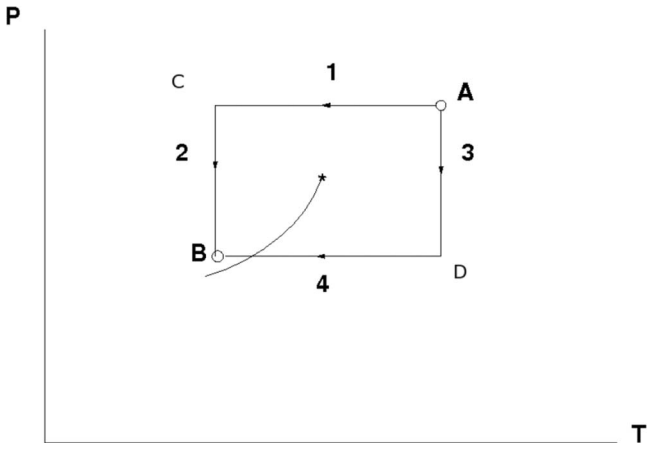

FIG. 6. Path for Monte Carlo calculations to determine the liquidus line.

nearest neighbor distances. Better matches of the experimental structure factors have been achieved with classical molecular dynamics models, but the classical models modify model parameters to fit the bulk liquid properties (as we did not do in the SCTB model) and of course the classical models give no description of aspects of the electronic and charge structure of the liquid which the SCTB code provides.

The model gives a dipole moment on an isolated water molecule of 1.96 Debye, whereas the average dipole moment in bulk water is calculated to be 2.3 Debye. The value for the liquid is somewhat smaller than value of 2.95 Debye obtained from a Car-Parinello simulation[19] and is (just barely) consistent with the reported experimental value of 2.9 ± 0.6 found from experiment.[20]

To estimate the vapor pressure line implied by the model, a molecular dynamics simulation was not feasible because the large latent heat and small simulation sample resulted in very large hysteretic effects. Instead, we used Monte Carlo simulations at fixed pressure and temperature (NPT ensemble). Some details of the method used, which differs from previous approaches, appear in Appendix C. The basic idea (Fig. 6) is to start at a pressure and temperature well above the critical point where the liquid and vapor are indistinguishable (point A in Fig. 6). Then we carry out a series of simulations determining the volume $V(P, T)$ and energy $E(P, T)$ (using the previous configuration as a starting point for each successive value of P, T) along two paths in the P, T plane to a point of interest (point B in Fig. 6). The two paths are chosen so that the fluid remains stably or metastably in the vapor phase along one path (A-3-D-4-B in Fig. 6) and in the liquid phase along the other path (A-1-C-2-B in Fig. 6). We then integrate the Gibbs-Duhem relation along the two paths using the simulation data to obtain values of the chemical potential at point B in the vapor phase and at point B in the liquid phase. If the two values are equal, then B is on the coexistence line. The method has the strong advantage of not requiring transfer of particles from one phase to another, as some other methods do.[21] As discussed in the Appendix C, however, the integration errors are substantial. In this way we determined the chemical potential within the model for both phases over a large region of the pressure/temperature phase space (50 atm $< P <$ 5000 atm, 100 °C $< T <$ 2500 °C) in a 96 water molecule simulation.

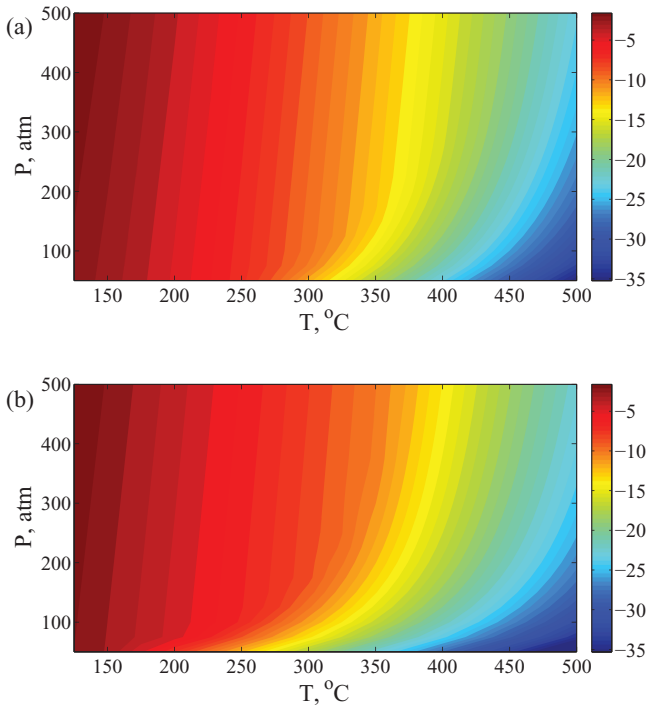

FIG. 7. Experimental values (a) and calculated values for the SCTB water model (b) of the chemical potential as a function of temperature and pressure. For the SCTB model, only the chemical potential for the phase with the lowest value of the chemical potential at a particular temperature and pressure is shown. The color intensity scale is in units of kJ/mol in both figures.

In Fig. 7, we show a comparison between the experimentally determined chemical potential of water[22] and the lowest calculated chemical potential for the SCTB water model (Appendix C) over the P, T plane. To make this direct comparison, we used the experimental value for entropy at $T = 500$°C and $P = 500$ atm, or 92.9 J/(mol · K) (point A in Figure 6) to fix a constant in the chemical potentials which is not determined by the calculation. (This is equivalent to choosing a reference state.) The calculated phase boundary is independent of this constant. We illustrate the determination of the phase boundary from the intersection of the calculated chemical potentials in Fig. 8.

The phase boundary found for the SCTB model is shown in Fig. 9, in which the experimental phase boundary (dashed line) is also provided for comparison. The major source of uncertainty in the phase boundary arose from the integration to find the change in entropy along the decreasing pressure leg of the vapor path. Although the location of the critical point is inaccessible using the formulation outlined in Appendix C, upper limits on the critical temperature and pressure could be determined by monitoring the Monte Carlo simulations. A jump to a large volume at a temperature of ~1000°C for pressures less than 1000 atm in simulations initially configured as a high-density liquid suggests that $T_C <$ 1000°C and $P_C <$ 1000 atm.

To study the melting line, we calculated, with SCTB MD, the mean square displacement $\langle \Delta^2 \rangle$ of oxygens in the water to determine the solid-liquid phase transition. If oxygens move

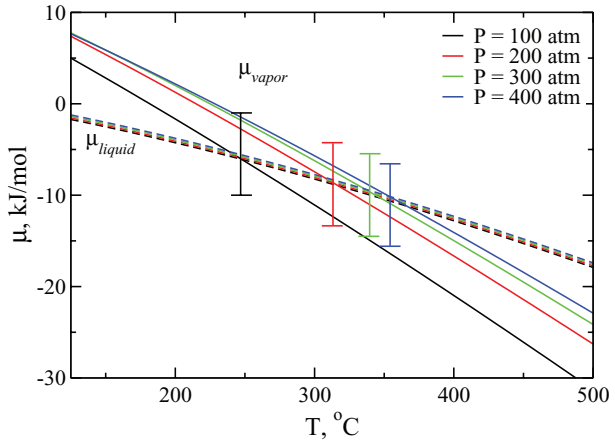

FIG. 8. Projections of the $\mu(P, T)$ surfaces onto the $\mu - T$ plane for various pressures showing the intersections which determine the coexistence line. The error bars indicate approximate numerical uncertainties, which arise mainly from the simulations of the chemical potential of the vapor phase.

diffusively, $\langle \Delta^2 \rangle = 6Dt$ where D is the diffusion constant and t is the time. Thus it is possible to compare our results to experimental ones. Experimental data from Ref. 23 show that $D = 2.30 \times 10^{-5}$ cm^2/s at ($T = 298$ K, $P = 1$ atm). The corresponding results are presented in Fig. 10. It appears that our SCTB diffusion constant at $T = 300$ K, $P = 1$ atm is 2.2094×10^{-5} cm^2/s which is very close to the experimental value. We can also see that the solid-liquid transition occurs between 250 K and 300 K at four different pressures we simulated. Therefore, we take the average of these two temperatures to get SCTB solid-liquid transition temperature. From these data, we constructed the phase diagram of SCTB water and by extrapolation, estimated the SCTB triple point as ($P = 0.00012$ atm, $T = 275$ K) which is close to the experimental result of ($P = 0.006$ atm, $T = 273.16$ K).

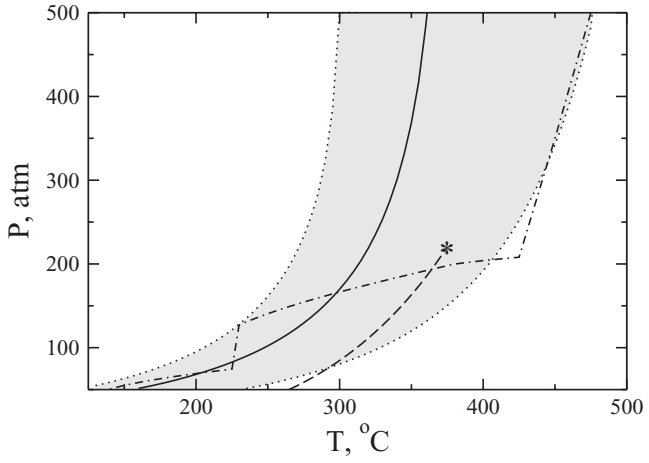

FIG. 9. The location of the liquid-vapor phase boundary for the SCTB water model (solid line) using the formulation described in Appendix C. The gray area denotes the uncertainty in this boundary. The experimental phase boundary is also shown (dashes), with an asterisk indicating the critical temperature and pressure. The results were obtained by calculating the chemical potential surfaces many times, finding the intersection, and averaging the results over runs. The shaded region is an estimate of the variance about this average. The dash-dotted line shows a result for the coexistence line from one run.

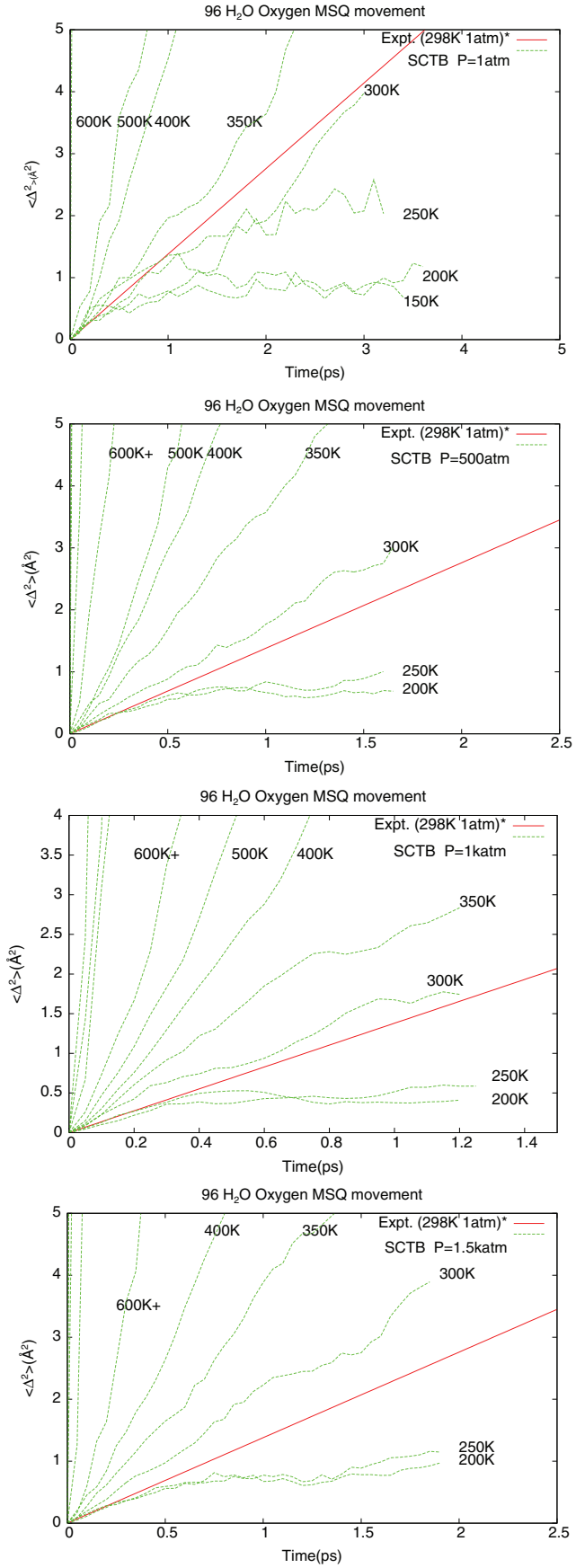

FIG. 10. Mean square displacement of water molecules in as calculated at various temperatures and pressures in the SCTB model with 96 water molecules.The red lines are obtained from the experimental value of the diffusion constant at 1 atm and 298 K.

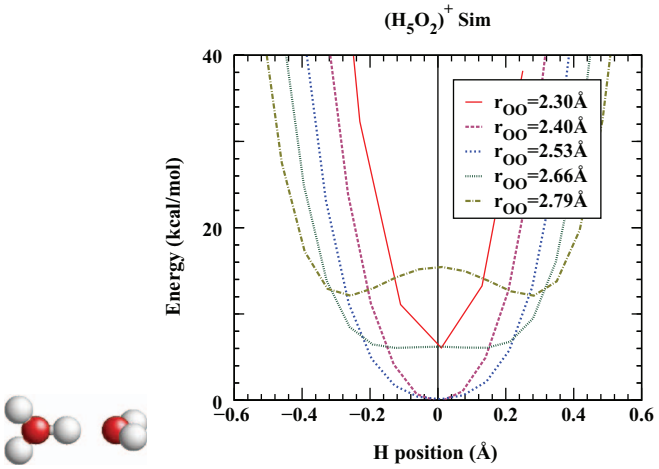

FIG. 11. Energy of a hydronium water cluster as a function of OO and OH distance.

However it is obvious that the uncertainties in the liquidus line render this a very rough estimate.

IV. WATER STRUCTURE AROUND A PROTON

In Figure 11, we show the result of calculation of the energy surface for the hydronium-water dimer (a 7 atom cluster) as a function of the oxygen-oxygen distance and the oxygen hydrogen distance (all other positions are allowed to relax). This energy surface, which was not fit, is quite similar to first principles ones[24] and, in particular, exhibits almost no barrier for H transfer from the hydronium to the water molecule. The binding energy of a gas phase hydronium ion to a water molecule is not expected to be quantitatively reproduced because the model was not fit for very large separations of water molecules. However, we find by holding the two oxygen positions fixed at a series of increasing separations while relaxing the hydrogen positions in the seven atom cluster that, for example, the energy increases by about 0.56 eV from the minimum at about 2.4 Å separation of the oxygens to 3 Å in the SCTB model, compared to an estimated first principles value of 0.86 eV from Ref. 24. (The value from Ref. 24 is not strictly comparable because the calculation included two additional water molecules.)

In the next two figures (Figs. 12 and 13) we compare results on the corresponding probability distribution of the proton in the H_3O_2 cluster in bulk water as simulated using a first principles Car Parinello method[25] and using SCTB. The results are qualitatively similar. The displacements of the proton from the midpoint between the oxygens is a little over 0.2 Å in the first principles calculation and a little over 0.1 Å in the SCTB calculation. The mean OO distance in the first principles calculation is around 2.48 Å and it is around 2.41 Å in the SCTB calculation. The curvature of the probability surface is lower in the first principles calculation than in the SCTB one.

V. ION TRANSPORT

To study proton transport in the model, we computed the conductivity in a system containing one proton, one hydroxyl, and 95 undissociated water molecules at 300 K. This is equivalent to 0.57 M(mol/liter) H^+ and OH^- concentration. The thermodynamic average of ion conductivity tensor σ is then calculated in the following way. For the small electric field $\mathbf{E}$, the current density $\mathbf{j}$ is

$$\mathbf{j} = \sigma \cdot \mathbf{E} = \frac{1}{Z\Omega} \sum_{ens} \left(\sum_i Q_i \mathbf{v_i} \right) e^{-\beta(H - \sum_j Q_j \mathbf{r_j} \cdot \mathbf{E})} = \frac{\beta}{\Omega} \int_0^\infty \left\langle \sum_{ij} Q_i \mathbf{v_i}(\mathbf{t} = \mathbf{0}) \mathbf{Q_j} \mathbf{v_j}(\mathbf{t}) \right\rangle \mathbf{dt} \cdot \mathbf{E}, \quad (3)$$

$$\sigma = \frac{\beta}{\Omega} \int_0^\infty \left\langle \sum_{ij} Q_i \mathbf{v_i}(\mathbf{0}) \mathbf{Q_j} \mathbf{v_j}(\mathbf{t}) \right\rangle \mathbf{dt}, \quad (4)$$

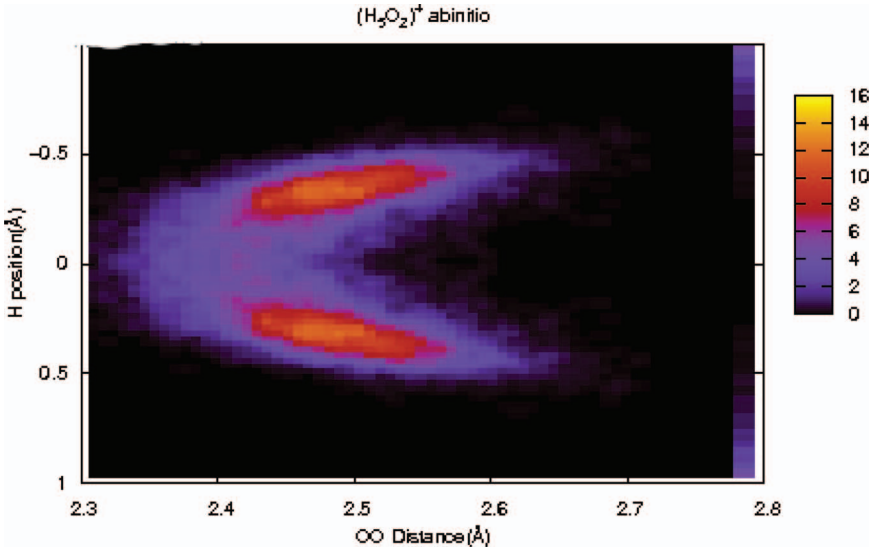

FIG. 12. First principles results for the relative proton positions in a Car-Parinello simulation for 32 water molecules and one proton.[25] Colors show the probability function $P(\delta, R_{OO})$ where $\delta = R_{O_aH} - R_{O_bH}$ relative to the O_aHO_b midpoint and R_{OO} is the distance between O_a and O_b.

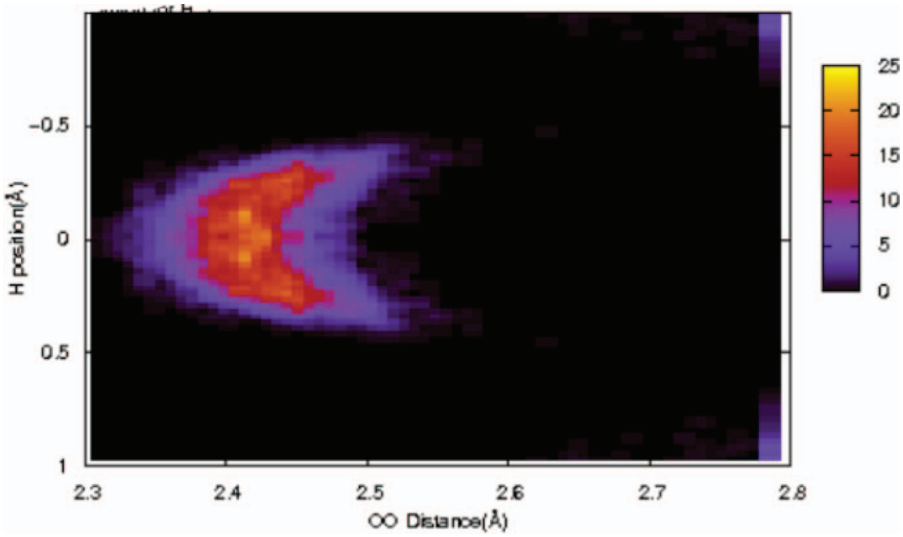

FIG. 13. Results for the relative proton positions in the SCTB simulation for 96 water molecules and one proton. As in the preceding figure, colors show the probability function $P(\delta, R_{OO})$ where $\delta = R_{O_aH} - R_{O_bH}$ relative to the O_aHO_b midpoint and R_{OO} is the distance between O_a and O_b.

where $\beta = 1/(k_BT)$ (k_B is Boltzman constant and T is temperature); Ω is the cell volume; $\sum_{ij}$ is the sum over all atoms in the unit cell; Q_i, $\mathbf{v_i}$, $\mathbf{r_i}$ are the charge, velocity, position of ith atom; t is the time; Z is the partition function; and "$\langle \cdot \rangle$" is a thermodynamic average. In an isotropic system such as liquid water, σ is diagonal and can be expressed as a scalar by taking the trace of the tensor

$$\sigma = \frac{\beta}{3\Omega} Tr \left(\int_0^\infty \left\langle \sum_{ij} Q_i \mathbf{v_i(0)} \mathbf{Q_j v_j(t)} \right\rangle \mathbf{dt} \right). \quad (5)$$

Instead of full summation over all atoms in the above expression, one can also take partial sums to obtain information concerning the contribution of different mechanisms of ion transport. For instance, for the water we study, in addition to the total ion conductivity, we calculated the following components of the frequency dependent conductivity: $\sigma_{HHtotal}$, σ_{HHself}, $\sigma_{HHnonself}$, where

$$\sigma_{HHtotal} =$$

$$\frac{\beta}{3\Omega} \int_0^\infty Tr \left(\left\langle \sum_{i\in H, j\in H} Q_i \mathbf{v_i(0)} \mathbf{Q_j v_j(t)} \right\rangle \right) e^{i2\pi f t} dt,$$

$$\sigma_{HHself} =$$

$$\frac{\beta}{3\Omega} \int_0^\infty Tr \left(\left\langle \sum_{i\in H} Q_i \mathbf{v_i(0)} \mathbf{Q_i v_i(t)} \right\rangle \right) e^{i2\pi f t} dt, \quad (6)$$

$$\sigma_{HHnonself} =$$

$$\frac{\beta}{3\Omega} \int_0^\infty Tr \left(\left\langle \sum_{i\in H, j\in H; i\neq j} Q_i \mathbf{v_i(0)} \mathbf{Q_j v_j(t)} \right\rangle \right) e^{i2\pi f t} dt,$$

where f stands for "frequency."

We collected data for 2.5 ps. The results are presented in Figure 14. The first picture shows components of the frequency dependent conductivity arising from "self" terms in the correlation function of the hydrogen velocity at one time with the hydrogen velocity at another time, and also the contribution from corresponding "non-self" hydrogen-hydrogen terms. Comparing these gives a measure of the contributions of self diffusion and Grotthuss-like contributions to the proton part of the conductivity. The second picture shows the calculated total conductivity and an extrapolation to zero frequency. The first picture indicates that $\sigma_{HHnonself}$ dominates σ_{HH}, so that the main contribution to the ion conductivity of a proton in this model of liquid water comes from a Grotthuss-like mechanism.[26,27] We used a parabola to fit the low frequency part of the ac ion conductivity and to extrapolate to zero frequency. We found that the total proton dc conductivity is 3.084 ± 0.34 s/cm; hydroxide contributes 1.852 ± 0.55 s/cm and the combined total dc ion conductivity from the SCTB model is 4.947 ± 0.56 s/cm. This is one order of magnitude higher than a recent experimental result of 0.3183 s/cm.[28] The ratio of the contribution from the proton and the hydroxide from SCTB is 1.6652, which is close to the experimental value of 1.7526.

VI. DISCUSSION

We have presented a SCTB model for water. It gives good structural properties of undissociated water except for some structure in the OH radial distribution function above 3.5 Å. The hydrogen bond is correctly described. The values of the liquid gas critical pressure, temperature, and concentration are also reasonably close to experimental ones, as is our estimate of the melting temperature. Our vapor pressure curve, obtained using a new Monte Carlo method, agrees with the experimental one within the (large) numerical uncertainties. The calculated value of the diffusion constant in undissociated water is quite close to the experimental one. With regard to the properties of protons in this model of water, we found

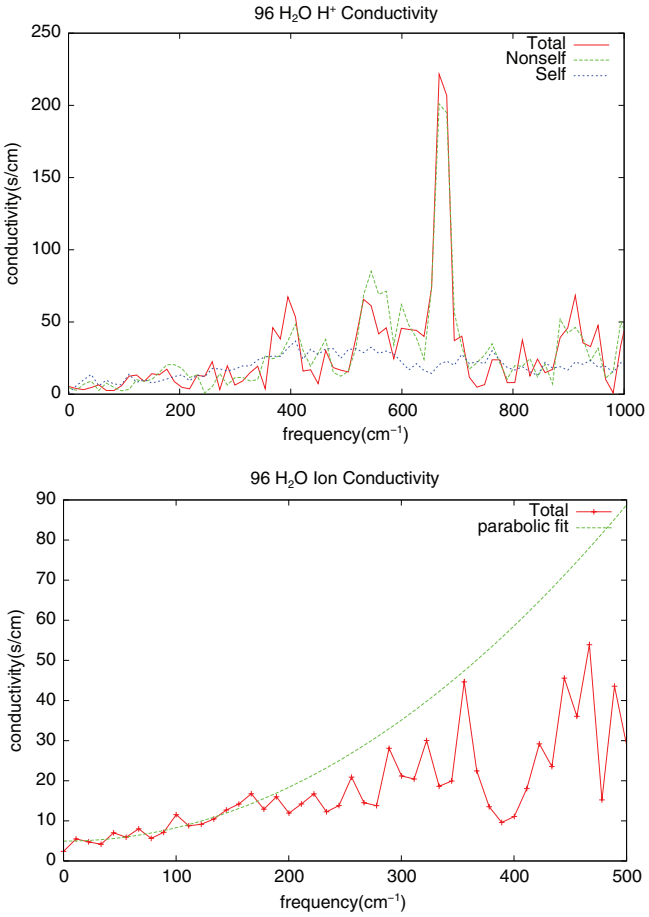

FIG. 14. Ion conductivity in 95 water and 1 H^+ and 1 OH^-. Top figure: Contributions to the AC conductivity from the hydrogen-hydrogen "self" terms in Eq. (6), from the hydrogen-hydrogen "nonself" terms and the sum of those two contributions. Bottom figure: The total ac conductivity (including contributions from charges on oxygen) and a fit to a parabola at low frequencies which was used to extrapolate to zero frequency.

semiquantitive agreement between the calculated structure of the water around a proton in this model and the calculations of Tuckermann *et al.*[25] With regard to transport, our calculations of the proton and hydroxyl conductivity in a system of 95 undissociated molecules and one dissociated one are consistent with a Grothuss-like mechanism, because the correlation function of unlike protons dominates the computed conductivity. The ratio of calculated proton to hydroxyl conductivity is in good agreement with experiment, but the total calculated ionic conductivity is about an order of magnitude too high compared to experiment.

Further comparisons of this model with known properties of water, such as the dipole moment per molecule at high temperatures and pressures,[29] are possible and will be the subject of future work.

This model can be run several orders of magnitude faster than full first principles Car-Parrinello and related methods using DFT direct dynamics. We believe that this can make it useful for study of properties which involve too many water molecules to allow first principles approaches. Furthermore, the calculations using SCTB can be further optimised, making the computation time advantage even larger, and we hope to report results on this aspect soon. By keeping the parameterization of oxygen the same in this model as in our previous model of titanium dioxide, we are able to use it to study titanium dioxide-water interfaces and we have reported results, using it, on the behavior of a nanoparticle of titanium dioxide in water.[10]

From the point of view of anticipated applications the most disappointing feature reported here is the order of magnitude discrepancy between the calculated ionic conductivity and the experimental one. However, a very small change in the activation energy for proton hopping across the hydrogen bond between a hydronium ion and a water molecule (Fig. 11) could account for this discrepancy, so it should be possible to correct for it by explicit fitting (which was not done here) in applications where this property is of particular importance.

ACKNOWLEDGMENTS

This work was supported by (U.S.) Department of Energy (DOE) (Grant No. DE-FG02-91ER45455) and by the University of Minnesota Supercomputing Institute. Pacific Northwest National Laboratories hosted a visit of J.W.H. during which this project was initiated. James Rustad is thanked for discussions.

APPENDIX A: SELF CONSISTENT TIGHT BINDING

The method is similar in some respects to those described in Refs. 13–15. We have noted the main differences between our SCTB method and others such as these in the introduction. The main idea in all these approaches is to use a small, localized basis set rather than the very large ones used in full first principles calculations in order to make the numerical calculations faster. Here we give a few technical details. Further details appear in Refs. 6 and 7. The energy, derived[30] by starting from first principles and making the Hartree Fock approximation for matrix elements of the coulomb interaction referring to orbitals on different sites, is taken to be

$$E = \sum_i E_i(Q_i, S_i^2, \{R\}) + \sum_{i,j,\nu,\nu'} Q_{i,\nu;j,\nu'}(v^{(1)}_{i,\nu;j,\nu'} + (1-\delta_{i,j})t_{i,\nu;j,\nu'}) + (1/2)\sum_{i\neq j}\frac{e^2(Z_i - Q_i)(Z_j - Q_j)}{\vec{R}_{ij}} - (1/2)\sum_{i\neq j,\nu,\nu'}\delta_{\sigma_\nu,\sigma_{\nu'}}\frac{e^2 Q^2_{j,\nu';i,\nu}}{R_{ij}} + \textit{multipole terms} \tag{A1}$$

where the indices ν, i refer to tight binding orbitals of type ν on site i. (The last term before the "multipole terms" accounts for exchange. It was not included in the water model described here.) $Q_{i\mu;j\nu}$ is the one particle density matrix in the tight binding basis, defined as

$$Q_{i\mu;j\nu} = \sum_\lambda n_\lambda c^*_{i\mu;\lambda} c_{j,\nu;\lambda}.$$

The coefficients $c_{i,\mu;\lambda}$ express eigenfunctions of the effective one electron equation derived from

$$\frac{\partial E}{\partial c^*_{i,\nu;\lambda}} = \epsilon_\lambda c_{i,\nu;\lambda}, \tag{A2}$$

in terms of the tight binding basis. In the general formulation,[30] the n_λ are eigenvalues of the one-particle density matrix which are determined here as "occupation numbers" set to 1 for the N lowest energy solutions to the effective one electron equation, which is solved self consistently. N is the total number of electrons. The "multipole terms" in the last equation are fully described in Ref. 6 except that we added dipole matrix elements between the tight binding basis states on the oxygen atoms to that formulation in order to allow the oxygen entities in the water model to develop a dipole moment (Table II).

In the description above, orbitals are taken to be orthogonal though , in practise, we solve the one electron equation in a nonorthogonal basis which involves overlap integrals $S_{i,\mu;j,\nu}$. Then E has a somewhat more complicated form[6] and we take the charge on site i to be

$$Q_i = \frac{1}{2}\sum_{\mu;j,\nu}(Q_{i,\mu,j,\nu}S_{i,\mu,j,\nu} + Q^*_{i,\mu,j,\nu}S^*_{i,\mu,j,\nu}). \quad \text{(A3)}$$

We also take

$$Q_{i,s} = \frac{1}{2}\sum_{\mu\in s;j,\nu}(Q_{i,\mu,j,\nu}S_{i,\mu,j,\nu} + Q^*_{i,\mu,j,\nu}S^*_{i,\mu,j,\nu}) \quad \text{(A4)}$$

to be the charge on site i associated with shell s. Parameters fixing the overlap integrals, the corresponding hopping matrix elements $t_{i\tilde{\nu},j,\tilde{\mu}}$ and the onsite functions $E_i(Q_i, S_i^2, \{R\})$ are varied to fit the results of first principles calculations. $E_i(Q_i, S_i, \{R\})$ is a function of the electronic charge Q_i of the ion at ion i, of the square of the total spin $S_i^2 = S_{ix}^2 + S_{iy}^2 + S_{iz}^2$ of the total spin of ion i and of the positions $\{R\}$ of the ions neighboring ion i (as well as of their charges, not written explicitly here). The functions $E_i(Q_i, S_i^2, \{R\})$ are chosen so that they describe the behavior of the isolated ions when the neighbors are far away. The quantities Q_i, S_i^2 in turn depend in a calculable way on the solutions to the one electron equation which is obtained by minimizing the energy with respect to the charge density, according to the Hohenberg-Kohn theorem leading to the set of effective one-electron equations (A2).

Solving these self consistently we get self consistent solutions for the charges, spins, and total energies of the system for any configuration of atoms. The interionic coulomb interactions are being treated in Hartree approximation but exchange and correlation effects of on site coulomb interactions are included through the functions $E_i(Q_i, S_i^2, \{R\})$. In this account, we have added a brief description of the treatment of spin dependence, not present in Ref. 6. More details on spin dependence appear in Ref. 12 where we showed that complex magnetic spin structures can be predicted by this method.[12] (In the application to water described in the present paper we did not include any spin dependence in the onsite terms.) For molecular dynamics, forces on each atomic site are determined by numerical evaluation of an expression obtained by differentiating the energy with respect to the position $\vec{R}_i$ of each ion i and then the atomic positions are moved according to the Verlet algorithm and the self consistent solution of the one electron equations is repeated, the forces are recalculated and so forth. In this way, the dynamics is following the approximate Born-Oppenheimer surface described by the self consistent tight binding model and all the dynamics are assumed to be adiabatic in that sense. Thus, in this implementation, we are making no attempt to account for cases, which can occur particularly near metal surfaces and in "level crossings" in chemical reactions, in which the time scales for electronic transitions are comparable to those for nuclear motion. In bulk water, where there is a large energy gap between the filled and empty eigenstates of the effective one electron equation, this neglect is justified.

APPENDIX B: SCTB PARAMETER SET FOR WATER

In practice, we use a non-orthogonal basis. There are three parts in the parameter space. To illustrate them clearly, we rewrite Eq. (A1) in the following way:

$$\begin{aligned} E = &\sum_i E_i(Q_i, S_i^2) + \sum_{i,\nu,j,\nu'} Q_{i,\nu;j,\nu'}(1-\delta_{i,j})t_{i,\nu;j,\nu'} \\ &+ \sum_{i,j,\mu(i\neq j)} E^{\{env\}}_{i,\mu}(R_{i,j})\sum_{j'\nu} Q_{i,\mu,j'\nu} \\ &+ Hartree\ terms + multipole\ terms. \end{aligned} \quad \text{(B1)}$$

The first part $E_i(Q_i, S_i^2)$ describes the properties of a single isolated atom. This term is only determined by the charge and spin of ion i. In the present application to water, we do not include any spin dependence. $E_i(Q_i, S_i^2)$ can then be written as the sum $\epsilon_{i,s}\sum_{\mu\in s}Q_{i,\mu} + E_{ion}(q)$. The letter "$s$" stands for "shell" and $q = Q_i - Z_i$ where Q_i is the Mulliken charge defined in Eq. (A3) and Z_i is the atomic number minus any core electrons. In the present water model, we treat the 1s oxygen orbitals as "core" so $Z_H = 1$, $Z_O = 6$. We call $\epsilon_{i,s}$ the "base energy" in our SCTB code, which is the energy of one-electron Hartree-Fock orbital of a neutral atom in shell "s". E_{ion} is the experimental ionization energy. This term is an empirical way of describing the local correlation and exchange effects. The second set of the parameters contains the hopping and overlapping terms. We apply the Slater two-center scheme[31] when parameterizing these terms. However, instead of the exponential form used in Refs. 6 and 30 we take the polynomial form for hopping terms $t_{i\mu;j\nu} = \sum_{n=4}^{13} t_n(\frac{r_0}{R_{ij}})^n$; and for overlaps $S_{i\mu;j\nu} = \sum_{n=4}^{13} s_n(\frac{r_0}{R_{ij}})^n$, where r_0 is a reference distance and R_{ij} is the distance between atom i and j. The final set of parameters describes the correlations and exchange interactions between atom i and its environment, which are called environmental terms in our code. We use a polynomial form like the one used for hopping and overlapping terms: $E^{\{env\}}_{i,\mu} = \sum_{n=4}^{13} a_n(\frac{r_0}{R_{ij}})^n$. The only multipole moment matrix element which is included in this water model is a dipole

TABLE I. Ionization potentials. $q = Q_i - Z_i$ where Q_i is the Mulliken charge defined in (A3) and Z_i is the atomic number minus the number of electrons in the core.

Atom	Ionization energy (eV)
Oxygen	$7.60367q + 5.25015q^2 - 0.0733333333q^3 + 0.820025q^4$
Hydrogen	$(.95 - .05q)(-13.6 - 0.757)/(e^{20.5219(q-0.62)} + 1.) + 13.6$

TABLE II. Multipole parameters.

	Oxygen	Hydrogen
$\langle s\|z\|p_z\rangle$	0.215 Å	0. Å

moment matrix element on the oxygen ions, as specified in Table II. In summary, we have $\epsilon_{i,\mu}$, the parameterization of $E_{ion}(q)$ in Table I, the dipole matrix element in Table II and the values of $\{t_n\}$, $\{s_n\}$ and $\{a_n\}$ in Tables III–V as the fitting parameters for SCTB model. "base energies" for each shell are $\epsilon_{O,2s} = -14.21\,eV$, $\epsilon_{O,2p} = 0.0$; $\epsilon_{H,1s} = 0.0$.

Altogether we are using 97 parameters to fit the first principles results in this model. However in order to assure compatibility with our previous SCTB model for titanium dioxide,[10] we did not vary the functional form or parameters describing the onsite energy of the oxygen ion or the form or parameters describing the overlap and kinetic energy matrix elements between orbitals on different oxygen ions. Fits which minimize the error function described in Eq. (1) with respect to the remaining parameters are carried out with a Monte Carlo code which conducts a random walk through the parameter space, retaining each new parameter set which reduces the error function (in the case of an effectively "zero temperature" fit). In the initial stages we introduce a finite "temperature" in the Monte Carlo algorithm to let the process get out of local minima in the error function and then lower the temperature for final adjustment. The fitting algorithms have been incorporated in a general "fitting code" which can use first principles cluster data (as in the application in this paper) or first principles data on cohesive energies and band structures of bulk solids (as was used for oxides[6] and metals[7,8] previously). The authors will make this and the direct dynamics SCTB code available on request.

We emphasize that the objective in this SCTB work is *not* to find a description with a minimal parameter set. Instead, we seek to minimize the basis size so that the resulting matrix diagonalizations, which must take place repeatedly inside the self consistency loop at each molecular dynamics step, will occur as rapidly as possible. These matrix diagonalizations, for which the required computation time scales with the cube of the matrix size, are the computational rate limiting step in the simulations. With the small basis set that we are using, fits to the first principles database require a large number of parameters, but this does not imply that there is much arbitrariness in the model. The first principles database is made large enough so that the parameter set is over constrained. Though we do not have proofs of the uniqueness of the fit, experience strongly suggests that there are not many, if any, other parameter sets which would give an equally good fit. In practise, the problem is not that we find multiple minima in the fitting process, but to find any reasonable fit at all.

TABLE IV. Overlapping parameters, $s_{i\mu;jv} = \sum_{n=4}^{9} a_n (\frac{r_0}{R_{ij}})^n$. Hopping terms have unit of eV, while overlapping terms have no unit. r_0 is different for different pairs: For O-O $r_0 = 2.50$ Å, O-H $r_0 = 0.96$ Å, H-H $r_0 = 1.50$ Å.

Overlapping	a_4	a_5	a_6	a_7	a_8	a_9
O-O						
$s_{ss\sigma}$	ZERO	0.051707	–0.223556	0.301365	–0.116977	
$s_{sp\sigma}$	ZERO	0.079783	–0.144048	–0.036584	0.069895	
$s_{pp\sigma}$	ZERO	0.029262	0.033281	–0.226318	0.131585	
$s_{pp\pi}$	ZERO	–0.010990	0.023468	–0.002940	–0.005215	
O-H						
$s_{ss\sigma}$	ZERO	9.505083	–20.168896	14.879056	–3.843764	
$s_{ps\sigma}$	ZERO	–10.434372	22.726173	–17.296037	4.529453	
H-H						
$s_{ss\sigma}$	ZERO	2.344369	–4.092163	2.494040	–0.542337	

APPENDIX C: MONTE CARLO METHODS

To find the gas liquid coexistence line in the model, the metastability of small molecular dynamics samples renders molecular dynamics an inappropriate method. Previous methods include simultaneous Monte Carlo simulation of the two phases in a Gibbs ensemble with provision for exchange of particles between phases.[21] Here we used a different method which does not require particle exchange. We use Monte Carlo simulations in the NPT ensemble. We describe some details of the Monte Carlo algorithm later in this Appendix. Assume in the present paragraph that the algorithm generates values of the volume and of the energy as a function of P and T. To determine the phase coexistence line (liquidus) we need to determine the chemical potentials $\mu_{liquid}(P, T)$ and

TABLE III. Hopping parameters, $t_{i\mu;jv} = \sum_{n=4}^{9} a_n (\frac{r_0}{R_{ij}})^n$. Hopping terms have unit of eV, while overlapping terms have no unit. r_0 is different for different pairs: O-O $r_0 = 2.50$ Å, O-H $r_0 = 0.96$ Å, H-H $r_0 = 1.50$ Å.

hopping	a_4	a_5	a_6	a_7	a_8	a_9	a_{10}
O-O							
$t_{ss\sigma}$	ZERO	–1.100143	4.735747	–6.402875	2.529529		
$t_{sp\sigma}$	ZERO	2.127806	–8.383724	10.474650	–3.884772		
$t_{pp\sigma}$	–3.465640	9.775484	–0.938716	–7.566228	–1.369081	6.599664	–2.290293
$t_{pp\pi}$	ZERO	–0.414364	1.684491	—2.167221	0.820618		
O-H							
$t_{ss\sigma}$	ZERO	–129.694743	279.683663	–208.263930	53.481483		
$t_{ps\sigma}$	ZERO	211.767103	–455.180710	337.533518	–85.332545		
H-H							
$t_{ss\sigma}$	ZERO	–16.334717	23.585237	–11.604696	2.039832		

TABLE V. Environmental parameters, $E_{i\mu;j} = \sum_n a_n (\frac{r_0}{R_{ij}})^n$. Unit eV. $r_0 = 1.95$ Å for all pairs.

	a_5	a_6	a_7	a_8	a_9	a_{12}
$O_{2s} \leftarrow O$	0.116311	0.203759	–1.693074	1.290759	0.306375	
$O_{2p} \leftarrow O$	0.116311	0.190202	–1.657808	1.316967	0.329593	
$O_{2s} \leftarrow H$	0.000103	0.000224	0.000320	0.001262	–0.000421	0.000002
$O_{2p} \leftarrow H$	0.000103	0.000222	0.000320	0.001259	–0.000422	0.000002
	a_6	a_7	a_8			
$H_{1s} \leftarrow H$	0.013608	0.010748	0.016658			

$\mu_{vapor}(P, T)$ and to solve the equation

$$\mu_{liquid}(P, T) = \mu_{vapor}(P, T).$$

We use paths in the P-T plane as illustrated in Figure 6. The point A is chosen to be well above the critical point, indicated by a *, where the gas and liquid phases are indistinguishable. Having obtained data on the volume $V(P, T)$ and energy $E(V, T)$ as a function of the pressure and the temperature from the Monte Carlo simulations, we then determine the chemical potential at point B, following the path A-1-2-B and again following the path A-3-4-B by integration of the Gibbs Duhem relation. The system is expected to remain in the liquid phase along the path A-1-2-B and in the vapor phase along A-3-4-B, no matter whether B is on the liquid or the vapor side of the liquidus line, because in the small simulation sample the phases will be metastable. However if B is on the coxistence curve, the chemical potentials will be found to be the same as calculated along the two paths so the position of the coexistence line can be located up to integration errors.

In a little more detail, the chemical potential difference is

$$\mu_B - \mu_A = \int_{path A\to B} (-s dT + v dP)$$

by the Gibbs-Duhem relation. s,v,e are S/N, V/N, E/N where N is the number of molecules. The second term is computed directly from $V(T, P)$ (and only legs 3 and 2 contribute to this term). The entropy along the paths is obtained from

$$\begin{aligned} s(P, T) = s(P_A, T_A) &- \int_{P_A}^{P} \left(\frac{\partial v(P', T}{\partial T}\right)_P dP' \\ &+ \int_{T_A}^{T} \left[(1/T')\left(\frac{\partial e(T', P_A)}{\partial T}\right)_P \right. \\ &\left. + (P_A/T')\left(\frac{\partial v(T', P_A)}{\partial T}\right)_P\right] dT' \end{aligned}$$

where we used $(\frac{\partial s}{\partial p})_T = -(\frac{\partial v}{\partial T})_P$ and $(\frac{\partial s}{\partial T})_P = (1/T)(\frac{\partial e}{\partial T})_P + (P/T)(\frac{\partial v}{\partial T})_P$. The chemical potential difference between the fluid at B and the fluid at A, calculated along the "vapor" path A→ D → B is then

$$\begin{aligned} &(\mu_B - \mu_D) + (\mu_D - \mu_A) \\ &= \int_{P_A}^{P_B} v(P, T_A) dP \\ &\quad + \int_{T_A}^{T_B} \left[-s(T_A, P_A) + \int_{P_A}^{P_B} \left(\frac{\partial v(P, T_A)}{\partial T}\right)_P dP\right] dT \\ &\quad - \int_{T_A}^{T_B} \left\{\int_{T_A}^{T} \left[(1/T')\left(\frac{\partial e(T', P_B)}{\partial T}\right)_P \right.\right. \\ &\quad \left.\left. + (P_B/T')\left(\frac{\partial v(T', P_B)}{\partial T}\right)_P\right] dT'\right\} dT. \end{aligned}$$

The first integral contributes along leg 3 and the second two integrals contribute along leg 4. In the second integral the integrand with respect to T has been obtained from an integral along path 3 to get the entropy at P_B, T_A. The integrand in this second term is constant with respect to temperature so it can be done analytically. The last term, contributing from path 4, contains a double integral on the temperature and evaluating this is a major source of numerical uncertainty in the method. The other main source of numerical uncertainty is the third term, involving $(\frac{\partial v(P, T_A)}{\partial T})_P$.

An essentially identical argument gives the chemical potential difference $\mu_B - \mu_A$ as evaluated along the "liquid" path path A → C → B:

$$\begin{aligned} &(\mu_B - \mu_C) + (\mu_C - \mu_A) \\ &= -\int_{T_A}^{T_B} \left\{s(T_A, T_B) + \int_{T_A}^{T} \left[(1/T')\left(\frac{\partial e(T', P_A}{\partial T}\right)_P \right.\right. \\ &\quad \left.\left. + (P_A/T')\left(\frac{\partial v(T', P_A)}{\partial T}\right)_P\right] dT'\right\} dT + \int_{P_A}^{P_B} v(P, T_B) dP. \end{aligned}$$

The first two terms contribute along leg 1 and the last term contributes along leg 2. In both expressions for the chemical potential, we have included a value $s(T_A, P_A)$ which cannot be evaluated from the simulation and depends on the reference state for the entropy. We adjust this as described in the text to make contact with experimental values.

Monte Carlo simulations at fixed pressure and temperature for both the liquid and vapor systems were averaged over a series of runs to determine the energy $e(T, P)$ and volume $v(T, P)$ surfaces. These surfaces were smoothed via least-squares, second-order polynomial fits. For the liquid systems, both the energy and volume surfaces were fit to polynomials that were second order in T and log (P). For the vapor system, in which there was a large variation in the volume over the temperature and pressure ranges, the logarithm of the volume was fit to a polynomial that was second order in log (P) and log (T), whereas the energy, as for the liquid system, was fit with a polynomial that was second order in T and log (P). Finally, for the vapor system, the entropy at the intersection of paths 3 and 4 was determined via individual fits of $v(T_A, P)$ at fixed temperature T_A along path 3 to reduce the error arising from this term. The results in Fig. 7(b) show only the

chemical potential associated with the phase calculated to have the lowest chemical potential at each value of pressure and temperature, whereas in Figure 8, we show the calculated chemical potentials for both phases to illustrate the method of determining the phase boundary.

Another detail concerns the volume dependence of the appropriate Metropolis weight for a Monte Carlo simulation in the NPT ensemble. The Gibbs potential is generally $G = F + P\langle V\rangle$ and, for fixed V the Helmholtz free energy F is

$$F = -k_B T \ln \int [d^N \mathbf{p}/(N!h^{3N})] d^N \mathbf{r} exp(-\mathcal{H}/k_B T).$$

Using $PV = -k_B T \ln e^{-PV/k_B T}$ and averaging over volumes at fixed P we obtain

$$G = -k_B T \ln \int V^{N-1}[dV/Ne] \int [d^N \mathbf{p}/(N!h^{3N})][d^N \mathbf{r}/V^N] \times exp(-(\mathcal{H} + PV)/k_B T)$$

in which the weights are chosen to give the right behavior in the ideal gas limit. The NPT ensemble is then reproduced by a Metropolis algorithm with the weighting factor for the probability of accepting state 2 when the simulation is currently in state 1 of

$$exp\big[+(1/k_B T)\big\{\mathcal{V}\big(r_1/V_1^{1/3}\big) - \mathcal{V}\big(r_2/V_2^{1/3}\big) + P(V_1 - V_2) - k_B T N \ln(V_1/V_2)\big\}\big]$$

when the argument of the exponent is negative (and 1 when the argument is positive). Here $\mathcal{V}(r/V_1^{1/3})$ is the system potential energy expressed in terms of the variables $\vec{r}_i/V^{1/3}$ and the volume V. The simulation is carried out using scaled coordinates $\vec{r}_i/V^{1/3}$ and varying the volume in the usual way. The last term in the exponential[32] is essential for a correct simulation of the vapor phase (though it is physically present in the liquid phase as well, but less important).

The merit of this alternative method for determining phase equilibrium is that it avoids the need for transferring particles between phases, which is numerically very cumbersome. As indicated in the body of the paper, the main deficiency is that it is difficult to control the numerical uncertainties associated with the integrations to obtain the entropy and the chemical potential.

[1] M. Krack, A. Gambirasio, and M. Parrinello, J. Chem. Phys. **117**, 9409 (2002).
[2] J. R. Rustad, J. W. Halley and A. Rahman, J. Chem. Phys. **98**, 4110 (1993).
[3] J. R. Rustad, B. P. Hay, and J. W. Halley, J. Chem. Phys. **102**, 427 (1995).
[4] A. Warshel, *Computer Modeling of Chemical Reactions in Enzymes and Solutions* (Wiley, 1991).
[5] S. Kamerlin *et al.*, J. Phys. Chem. **113**, 10905 (2009).
[6] P. K. Schelling J. W. Halley, and N. Yu, Phys. Rev. B **58**, 1279 (1998).
[7] S. Erdin, Y. Lin, and J. W. Halley, Phys. Rev. B **72**, 035405 (2005).
[8] A. Tchernatinsky and J. W. Halley, Phys. Rev. B **83**, 205431 (2011).
[9] Y. Lin, Ph.D. dissertation, University of Minnesota, 2011.
[10] J. W. Halley, S. Erdin, Y. Lin, and P. Zapol, J. Electroanal. Chem. **607**, 147 (2007).
[11] A. T. Paxton and J. J. Kohanoff, J. Chem. Phys. **134**, 044130 (2011).
[12] M. Zhuang and J. W. Halley, Phys. Rev. B **64**, 24413 (2001).
[13] M. Kohyama, S. Kose, M. Kinoshita, and R. Yamamoto, J. Phys.: Condens. Matter **2**, 7791 (1990).
[14] J. A. Majewski and P. Vogel, Phys. Rev. B **35**, 9666 (1987).
[15] M. Elstner, D. Porezag, G. Jungnickel, J. Elsner, M. Haugk, T. Frauenheim, S. Suhai, and G. Seifert, Phys. Rev. B **58**, 7260 (1998).
[16] J. Ortega, J. P. Lewis, and O. F. Sankey, Phys. Rev. B **50**, 10516 (1994).
[17] A. K. Soper and M. G. Phillips, Chem. Phys. **107**, 47 (1986).
[18] J. M. Sorenson, G. Hura, R. M. Glaeser, and T. Head-Gordon, J. Chem. Phys. **113**, 9149 (2000).
[19] P. L. Silvestrelli and M. Parrinello, Phys. Rev. Lett. **82**, 3308 (1999).
[20] Y. S. Badyal, M.-L. Saboungi, D. L. Price, S. D. Shastri, D. R. Haeffner, and A. K. Soper, J. Chem. Phys. **112**, 9206 (2000).
[21] A. Z. Panagiotopoulos, N. Quirke, M. Stapleton, and D. J. Tildesley, Mol. Phys. **63**, 527 (1988).
[22] W. Wagner and A. Pruss, J. Phys. Chem. Ref. Data **31**, 387–535 (2002).
[23] K. T. Gillen, D. C. Douglass, and M. J. R. Hoch, J. Chem. Phys. **57**(12), 5117 (1972).
[24] S. Scheiner, J. Am. Chem Soc. **103**, 315 (1981).
[25] D. Marx, M. Tuckerman, J. Hutter, and M. Parrinello, Nature (London) **397**, 601 (1999).
[26] C. J. T. de Grotthuss, Ann. Chim. **58**, 5473 (1806).
[27] T. C. Berkelbach, H.-S. Lee, and M. E. Tuckermann, Phys. Rev. Lett. **103**, 238302 (2009).
[28] T. S. Light, S. Licht, A. Bevilacqua, and K. R. Morash, Electrochem. Solid-State Lett. **8**, E16 (2005).
[29] D. Kang, J. Dai, and J. Yuan, J. Chem. Phys. **135**, 024505 (2011).
[30] N. Yu and J. W. Halley, and N. Yu, Mater. Sci. Forum **185–188**, 389 (1995).
[31] J. C. Slater and G. F. Koster, Phys. Rev. **94**, 1498 (1954).
[32] M. P. Allen and D. J. Tildesley, *Computer Simulation of Liquids* (Clarendon Press, Oxford, 1987), p. 124.